Developments in the Built Environment 24 (2025) 100775

Contents lists available at ScienceDirect

Developments in the Built Environment

journal homepage: www.sciencedirect.com/journal/developments-in-the-built-environment

# Influence of thermally activated artificial concrete fines composition on mortar strength development

Jan P. Höffgen *, Frank Dehn

*Karlsruhe Institute of Technology (KIT), Institute for Concrete Structures and Building Materials (IMB), Gotthard-Franz-Str. 3, Karlsruhe, 76131, Germany*

ARTICLE INFO

*Keywords:*
Concrete
Cement
Mineral waste
Recycling
Thermal activation
Supplementary cementitious material

ABSTRACT

The study explores the use of thermally activated concrete fines as substitution for cement to recycle mineral waste and reduce emissions. Concrete fines from waste recycling have a significant impact on compressive strength, with considerable variation due to their varying compositions. In the present study, 12 artificial concrete fines with varying compositions are thermally activated and assessed for their strength contribution. Increasing aggregate content within artificial fines results in a decrease in compressive strength, with aggregate mineralogy and binder composition having a major impact. Ultimately, this study proposes a model for predicting the impact of fines composition on compressive strength based on mass loss during dehydration. For thermally activated cement paste, the new model proposes no influence on compressive strength compared to the reference ($k = 1.0$). Paste precursors containing hydration products from alternative binders may even surpass the reference ($k > 1.0$), while an increasing amount of inert aggregates reduces strength ($k < 1.0$).

## 1. Introduction

Concrete is essential for the production of infrastructure and housing, but faces challenges: The sourcing of aggregates already results in localized shortages, and the production of cement clinker as a hydraulic binder entails high $CO_2$-emissions (VDZ, 2024; Coffetti et al., 2022). Therefore, concrete and composite cements partially substitute clinker through supplementary cementitious materials (SCMs), or even avoid cement altogether as alkali-activated materials (Coffetti et al., 2022; Gao et al., 2013; Knight et al., 2023; Barthel et al., 2016; Shah et al., 2022; Herrmann et al., 2018; Wang et al., 2024; Ma et al., 2025; Wu et al., 2024). However, some of the most widely used SCMs – ground granulated blast-furnace slag and coal fly ash – already face regional shortages, which will only magnify when less coal is burned in steel production and power plants, thus raising the need for the identification of additional SCMs (Hafez et al., 2020; Knight et al., 2023; Snellings et al., 2023; Friol Guedes de Paiva et al., 2021).

Concrete recycling may provide an alleviation for both issues. However, while the application of recycled concrete aggregates is well established, cement recycling requires additional research and development. One pathway for cement recycling is thermal activation, where hydrated cement paste (HCP) retains reactivity after the loss of chemically bound water (Carriço et al., 2020a; Ohemeng and Ekolu, 2020; Xu et al., 2022; Aquino Rocha and Toledo Filho, 2023; Zheng et al., 2024). HCP mostly consists of cement clinker hydration products, namely calcium silicate hydrate and calcium hydroxide from the hydration of tricalcium silicate ($C_3S$) and dicalcium silicate ($C_2S$), as well as aluminous, ferrous, or sulfate hydrates (Richardson, 2000; Scrivener et al., 2015). The hydration of 1 g of ordinary Portland cement (OPC) requires about 0.4 g of water, of which 0.2 g–0.25 g is chemically bound in hydrates (Lura et al., 2017; Powers and Brownyard, 1946; Brouwers, 2004). The remainder is present as physically bound water in gel pores. While the latter evaporates at temperatures up to 105 °C, the disintegration of different hydraulic phases in HCP requires increased temperatures (see Table 1). Calcium silicate hydrate is transformed into reactive $\alpha'_L C_2S$ and $\alpha'_H C_2S$, with calcium oxide to silicon dioxide ratios ranging between 1.73 and 1.9 (Bogas et al., 2022b; Alonso and Fernandez, 2004; Richardson, 2000; Ge et al., 2024; Noel et al., 2025; Tajuelo Rodriguez et al., 2017; Carriço et al., 2020b; Real et al., 2020; Serpell and Zunino, 2017). Dehydrated cement paste (DCP) exhibits high specific surface areas and high porosity, which originates in porous HCP and increases with increasing temperature and phase decomposition (Baldusco et al., 2019; Bogas et al., 2019; Carriço et al., 2020b; Kim et al., 2021). For processing temperatures surpassing the dehydroxylation range of calcium hydroxide, DCP may contain finely distributed calcium oxide (Bogas et al., 2019; Serpell and Lopez, 2015).

When used as a recycled binder, rehydration begins with the reformation of calcium hydroxide from calcium oxide, and the reformation of calcium silicate hydrates from $C_2S$, which manifests in increased and

* Corresponding author.
*E-mail address:* jan.hoeffgen@kit.edu (J.P. Höffgen).

https://doi.org/10.1016/j.dibe.2025.100775
Received 13 August 2025; Received in revised form 29 September 2025; Accepted 4 October 2025
Available online 13 October 2025

**Table 1**
Temperature-dependent decomposition of concrete fines containing hardened cement paste and aggregates.
*Source:* Data from (Angulo et al., 2022; Baggio et al., 2024; Baldusco et al., 2019; Baquerizo et al., 2016; Florea, 2014; Horváth et al., 1977; Klingsch, 2014; Schneider, 1982; Wang et al., 2019; Zelic et al., 2007; Zhou and Glasser, 2001; Zhou et al., 2004).

| Temperature [°C] | | | Process |
|---|---|---|---|
| | < | 105 | Loss of free and physically bound water |
| | < | 115 | Disintegration of ettringite |
| | < | 250 | Disintegration of monosulfate |
| 260 | – | 400 | Decomposition of calcium aluminate hydrates |
| 110 | – | 500 | Disintegration of calcium silicate hydrates |
| 400 | – | 550 | Dehydroxylation of calcium hydroxide |
| | 573 | | Quartz inversion in siliceous aggregates |
| 650 | – | 900 | Calcination of carbonated cement phases or carbonatic aggregates |

accelerated hydration heat development (Angulo et al., 2022; Bogas et al., 2020; Semugaza et al., 2023; Yu and Shui, 2013; Wei et al., 2025; Baldusco et al., 2019; Real et al., 2020). However, due to the porous nature of DCP, rehydrated C–S–H forms inside the particles, and exhibits weak interparticle connectivity after hydration, resulting in a low-strength material (Carriço et al., 2020b; Shui et al., 2008; Real et al., 2020; Xi et al., 2024a). Yet, when used as SCM, water consumption of DCP reduces the available water for clinker hydration, which forms a dense and interlocking microstructure (Qian et al., 2020; Tokareva et al., 2023; Wei et al., 2025). Small amounts of thermally activated cement paste may have a positive impact on compressive strength (Ma et al., 2022; Wei et al., 2025; Carriço et al., 2021b). However, with increasing substitution rate, strength declines (Carriço et al., 2020b; Semugaza et al., 2023). Overall, up to 40 wt% of clinker can be substituted through DCP with minimal adverse effects on concrete strength (Bogas et al., 2022a; Carriço et al., 2020b; Letelier et al., 2017; Ma et al., 2022; Qian et al., 2020; Tokareva et al., 2023; Vashistha et al., 2023; Wu et al., 2023).

When HCP contains hydration products from pozzolanic or latent-hydraulic SCMs, like fly ashes or ground granulated blast-furnace slag, dehydration and rehydration behavior changes. Prominently, the reduction of clinker reduces the amount of calcium hydroxides in HCP, in favor of an increased amount of calcium silicate hydrates and calcium aluminate silicate hydrates (Xu et al., 2023b). After processing, the rehydration potential increases, especially for ground granulated blast-furnace slag containing cement paste, which shows increased hydration heat development and higher compressive strength (Xu et al., 2023b,a). HCP containing fly ash exhibits reduced hydration heat and compressive strength, while inert limestone powder as part of SCM merely dilutes DCP performance, as long as the processing temperature is kept below calcination temperature (Xu et al., 2023b,a; Serpell and Lopez, 2013). While the dehydration and rehydration of HCP from OPC have been thoroughly investigated, the behavior of HCP from binary cements lacks a detailed analysis.

Similar shortcomings concerning the influence of aggregate type and content in recycled concrete fines need addressing. Fines from waste concrete processing never consist of pure HCP and always contain primary aggregates, which have an overall negative impact on performance as SCM following thermal activation (Bogas et al., 2019; Carriço et al., 2021a,b). However, the mineral composition of finely ground aggregates impacts their performance as SCM, especially when containing amorphous silicon dioxide, which exhibits a pozzolanic reactivity (Lipowsky and Müller, 2017). Regardless, no studies where the influence of aggregate type and concentration was assessed employing artificial fines could be identified.

Therefore, this study presents a systematic approach for assessing the influence of concrete fines composition regarding cement composition and aggregate content on the performance of thermally activated concrete fines as SCM.

**Table 2**
Composition of artificial fines used as precursors for thermal activation. $w/b$: water-binder ratio; $v_p$: paste volume; A: aggregates; FA: fly ash; S: blast-furnace slag; RS: river sand; LS: limestone sand; GW: greywacke.

| | Binder | $w/b$ | $v_p$ [v%] | A |
|---|---|---|---|---|
| CEM | 100 wt% CEM I | 0.5 | 100 | – |
| RS75 | 100 wt% CEM I | 0.5 | 75 | RS |
| RS62 | | | 62.5 | |
| RS50 | | | 50 | |
| LS75 | 100 wt% CEM I | 0.5 | 75 | LS |
| LS50 | | | 50 | |
| GW75 | 100 wt% CEM I | 0.5 | 75 | GW |
| GW50 | | | 50 | |
| FA0 | 70 wt% CEM I + 30 wt% FA | 0.5 | 100 | – |
| FA50 | | | 50 | RS |
| S0 | 70 wt% CEM I + 30 wt% S | 0.5 | 100 | – |
| S50 | | | 50 | RS |

**Table 3**
Mix designs of artificial fines used as precursors for thermal activation [g/l]. W: Water; C: CEM I 42.5 R; FA: fly ash; S: blast-furnace slag; RS: river sand; LS: limestone sand; GW: greywacke.

| [g/l] | W | C | FA | S | RS | LS | GW |
|---|---|---|---|---|---|---|---|
| CEM | 610 | 1220 | | | | | |
| RS75 | 458 | 915 | | | 658 | | |
| RS62 | 381 | 763 | | | 986 | | |
| RS50 | 305 | 610 | | | 1315 | | |
| LS75 | 458 | 915 | | | | 670 | |
| LS50 | 305 | 610 | | | | 1340 | |
| GW75 | 458 | 915 | | | | | 678 |
| GW50 | 305 | 610 | | | | | 1355 |
| FA0 | 583 | 816 | 350 | | | | |
| FA50 | 292 | 408 | 175 | | 1315 | | |
| S0 | 605 | 847 | | 363 | | | |
| S50 | 303 | 424 | | 182 | 1315 | | |

## 2. Experimental program

The experimental program aims to assess the influencing parameters of concrete fines composition on the performance as supplementary cementitious materials. Thermally activated artificial fines were assessed for their rehydration behavior and compressive strength development.

### 2.1. Materials

To reflect the bandwidth of possible concrete fines from existing or demolished concrete structures, 12 artificial fines with known compositions were produced. Variations include aggregate composition and content as well as the partial substitution of OPC (CEM I 42.5 R, "CEM I") through reactive supplementary cementitious materials. Table 2 gives an overview of the artificial fines compositions and naming scheme. Table 3 details the corresponding mix designs.

The basis of the artificial fines is hardened cement paste (HCP) made from CEM I 42.5 R. The influence of the type of sand is to be investigated primarily on mortars with an aggregate content of 50 v%. A quartzitic river sand (RS) and a calcitic crushed limestone sand (LS), which are intended to represent the predominantly used types of aggregate, are used. In addition, two artificial fines were produced with greywacke (GW), whose alkali reactivity was known from a previous research project (Wiedmann, 2020). To investigate the influence of the aggregates content, additional artificial fines with an aggregates content of 25 v% – and in the case of RS 37.5 v% – were produced. Since the use of OPC has been declining in recent years, pure binder pastes and mortars with an aggregates content of 50 v% by volume, in which 30 wt% of CEM I was replaced by fly ash (FA) or ground

granulated blast-furnace slag (S), which are widely used pozzolanic or latent-hydraulic SCMs, complete the artificial fines matrix.

All artificial fines were manufactured with a fixed water-binder ratio of $w/b = 0.5$, as it can be assumed that at $w/b = 0.5$, the entire binder is hydrated, even if the local $w/b$-ratio may be slightly altered. Preliminary analyses showed that lower $w/b$-ratios were feasible for the production of paste materials, but required the undesired addition of superplasticizer for mortars with low paste content. Higher $w/b$-ratios, as often found in practice, do not lead to an increased degree of hydration, but affect the porosity of the cement matrix. On the other hand, the tendency of the fresh mortar to segregate increases with increasing $w/b$-ratio, especially with high paste content. Pure paste artificial fines (CEM, FA0, S0) nonetheless showed segregation, so these materials were repeatedly homogenized by hand after the original mixing until hydration had started. From all artificial fines, prisms ($(20 \times 20 \times 80)\,mm^3$) for strength testing were cast.

Bulk artificial fines were stored in sealed buckets to ensure a high degree of hydration. Prisms were demolded at 1 d and subsequently stored under water alongside bulk samples until the age of testing at 2 d, 7 d, 28 d, and 356 d. At an age of at least 9 months, bulk specimens were crushed and dried at 105 °C, followed by grinding in an industrial mill. Ground and dried artificial fines were labeled with the suffix "−100". Subsequent thermal activation used a static oven with a crucible size of 1.5 kg. The thermal activation procedure was obtained from preliminary analyses, with a heating rate of 5 K/min and a holding time of 6 h at the individual processing temperature (400 °C, 600 °C or 800 °C), before cooling in laboratory climate. Afterwards, samples were stored in a sealed container containing a drying agent. Similar to ground artificial fines, the naming scheme for thermally activated samples added the temperature as a suffix to the artificial fines, i.e., "GW75-400" for a mortar containing 25 v% greywacke, which was activated at 400 °C.

The artificial fines matrix was complemented by RS0 and LS0, which denote the respective aggregates used for mortars, after grinding in a laboratory mill.

### 2.2. Experimental procedures

Raw materials as well as artificial fines were characterized for their chemical composition through Wavelength Dispersive X-ray Fluorescence (WDXRF), their particle size distribution, and density. The thermal decomposition behavior of artificial fines was assessed through thermogravimetric analyses before and after activation (sample sizes: 160 mg, heating rate: 10 K/min).

Isothermal hydration heat measurements were conducted on blends of CEM I and artificial fines at 20 °C with internal mixing, enabling the determination of the initial heat release. Preliminary tests on mixing efficiency and homogeneity led to setting the water-binder ratio to $w/b = 0.6$ for all samples. Artificial fines were generally investigated in combination with CEM I at a substitution rate of $f = 0.3$. Double determinations were performed for all mixes, except for the base mix with pure CEM I, which comprised eight single measurements. Additionally, activated paste artificial fines (CEM, FA0, S0) were tested at different CEM I-substitution rates.

For strength development tests, a mortar with 50 v% quartzitic river sand (0 mm–2 mm) as aggregates was used, matching the composition of RS50. To assess the influence of artificial fines on SCM, two mixes with $w/b = 0.4$ and $w/b = 0.5$ at $f = 0.3$ were produced for each SCM, with selected SCMs also having $w/b = 0.5$ at $f = 0.1$ and $f = 0.5$. Fourteen base mixes with pure CEM I were produced with $w/b = 0.40$–$0.65$ and were repeated in three series throughout the experimental program. 159 mixes, including repetitions, were tested for the assessment of CEM I-substitution through processed artificial fines. In stiff mortars, superplasticizer was added to ensure comparable workability. After mixing, the mortar was placed in steel molds, which were moist-cured for 1 d, and then stored underwater at 20 °C after demolding. Strength testing was performed on three prisms each ($(20{\times}20{\times}80)\,mm^3$) at 2 d and 28 d. The small specimen size (half of a standard mortar prism according to EN 196:2016) was chosen for the reduced amount of raw materials required for one mix. This allowed for the production of up to four different mortar compositions from one batch of thermally activated artificial fines. For CEM I, as well as CEM and different RS-artificial fines, additional strength measurements were conducted at 1 d and 7 d. First, flexural strength $f_f$ was determined with a span of 50 mm at a loading rate of $\dot{F}_f = 10\,N/s$. Compressive strength ($f_c$) testing used six prism halves at a loading rate of $\dot{F}_c = 600\,N/s$.

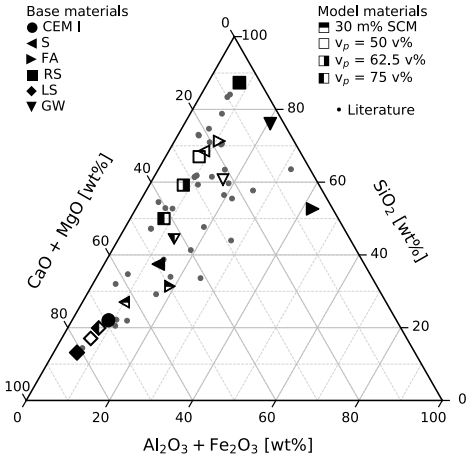


**Fig. 1.** Ternary illustration of raw materials and artificial fines composition determined through WDXRF (EN 196-2:2013) as well as literature (Baggio et al., 2024; Chen et al., 2024; Gebremariam et al., 2020; Kim and Ubysz, 2024; Sousa et al., 2024; Tokareva et al., 2023; Vashistha et al., 2023; Sui et al., 2020; Wei et al., 2024, 2025; Xi et al., 2024b; Yonis et al., 2024; Zhang et al., 2023; Cyr et al., 2019; Florea, 2014; Frías et al., 2021; Brameshuber et al., 2011; Izoret et al., 2019; Li et al., 2021; Liang et al., 2021; Liu et al., 2021; Müller and Dora, 2000; Shen et al., 2021; Sun et al., 2021). See Table 2 for artificial fines composition.

## 3. Results and discussion

### 3.1. Precursors characterization

Table 4 lists the results of the strength development of artificial fines prisms. Overall, strength increases with reduced paste content, while aggregate composition does not exhibit a systematic influence. Materials, where CEM I was partially substituted through reactive SCMs, show a slower strength development, but exhibit similar 356 d-compressive strength as equivalent materials without CEM I-substitution, with S50 reaching the highest ultimate compressive strength of all artificial fines prisms.

Fig. 1 illustrates the chemical composition of raw and artificial fines in a ternary diagram. Results show the expected difference between individual artificial fines.

The chemical composition reflects variations between individual RCFs from the literature, which consist of different kinds of binders and aggregates. Fig. 1 also implies that the chemical composition is not suited as a standalone assessment parameter of RCF potential.

The thermal behavior of artificial fines was determined on samples that had been dried at 105 °C to eliminate free and physically bound water. Instead of industrial grinding, samples were ground in a laboratory ball mill immediately after drying (Fig. 2).

Here, the influence of the type and content of the aggregates is shown, which is in good agreement with the XRF results. Regardless of aggregate composition, mass loss up to 600 °C scales with paste content, as pure aggregates exhibit almost no mass loss for lower temperatures. Mass loss of artificial fines with different aggregate types

**Table 4**
Flexural ($f_f$) and compressive strength ($f_c$) of artificial fines prisms at 2 d, 7 d, 28 d and 365 d on prisms with $(20 \times 20 \times 80)\,mm^3$.

| | $f_f$ at the age of | | | | $f_c$ at the age of | | | |
|---|---|---|---|---|---|---|---|---|
| | 2 d | 7 d | 28 d | 365 d | 2 d | 7 d | 28 d | 365 d |
| CEM | 4.6 | 7.1 | 7.4 | 8.1 | 20.3 | 36.8 | 42.5 | 53.6 |
| RS75 | | 7.4 | 8.5 | 8.5 | | 38.7 | 46.7 | 55.9 |
| RS62 | 6.0 | 8.0 | 8.6 | 6.3 | 27.1 | 46.1 | 50.4 | 53.6 |
| RS50 | 6.1 | 7.7 | 8.5 | 8.9 | 26.5 | 48.3 | 50.0 | 60.5 |
| LS75 | | 6.7 | 7.1 | 7.4 | | 41.5 | 45.6 | 53.1 |
| LS50 | 6.2 | 7.9 | 8.7 | 10.1 | 29.7 | 49.8 | 56.5 | 64.1 |
| GW75 | | 7.0 | 8.6 | 7.9 | | 43.0 | 50.4 | 60.3 |
| GW50 | 6.1 | 8.3 | 9.9 | 11.2 | 32.9 | 52.8 | 47.6 | 65.4 |
| FA0 | 2.8 | 4.4[a] | 6.7 | 9.2 | 11.0 | 22.9 | 35.1 | 56.8 |
| FA50 | 3.9 | 5.6 | 5.7 | 9.6 | 18.0 | 32.9 | 37.9 | 56.6 |
| S0 | 3.8 | 4.5[a] | 7.2 | 8.9 | 13.3 | 24.2 | 37.4 | 53.9 |
| S50 | 4.6 | 6.9 | 8.9 | 11.2 | 21.8 | 39.0 | 54.3 | 73.8 |

[a] At 7 d, FA0 and S0 were tested with $\dot{F}_f = 1\,N/s$.

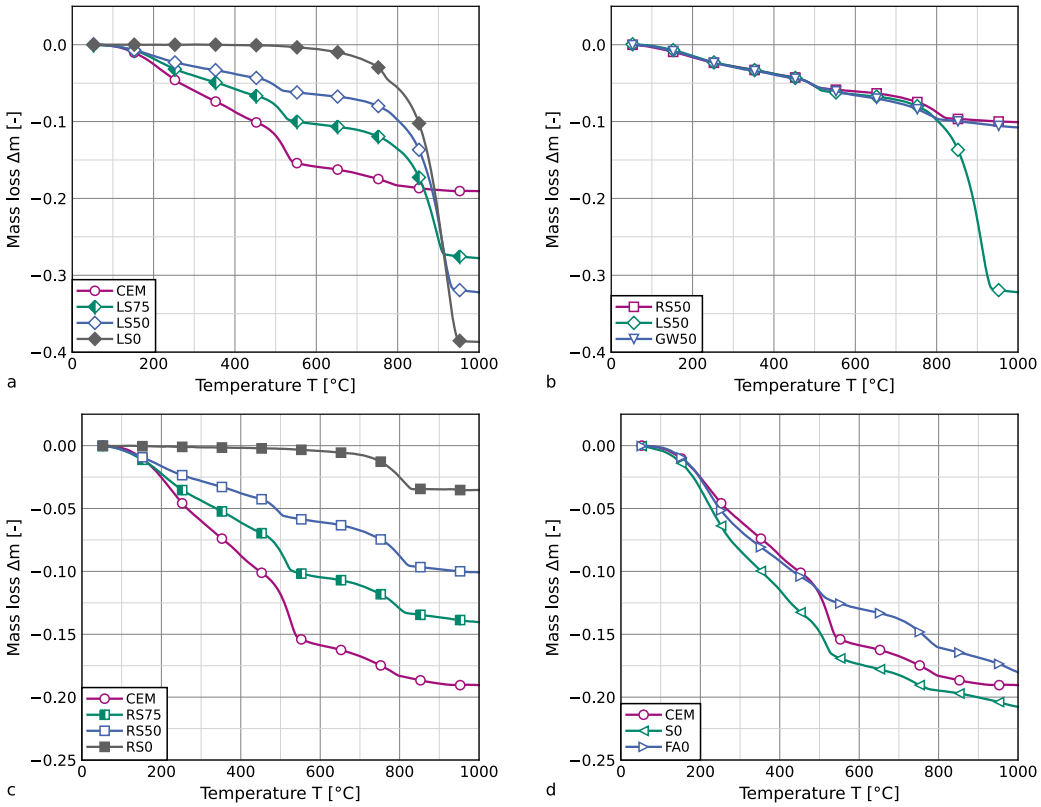


**Fig. 2.** Thermogravimetric characterization of artificial fines (sample size 160 mg, heating rate 10 K/min). See Table 2 for artificial fines composition.

but the same aggregate content is almost identical. The artificial fines with limestone aggregate (LS) show a high mass loss at temperatures above 810 °C, which is only slightly present in the artificial fines with greywacke and not present in samples with siliceous river sand. This is due to the decomposition of calcium carbonate ($CaCO_3$) in the aggregate particles. However, all artificial fines exhibit a mass loss between 700 °C and 800 °C, which is also caused by the decomposition of calcium carbonate. The different decomposition temperatures can be explained by different mineralogical and petrographic compositions or configurations of $CaCO_3$.

In addition to the obvious influence of the aggregate content on the mass loss, Fig. 2 also shows differences between cement pastes with different binder compositions. FA0, in which 30 wt% of the hydraulically reactive CEM I was replaced by pozzolanic coal fly ash, shows a similar mass loss up to temperatures of around 500 °C as CEM. However, the subsequent increased mass loss, which is due to the decomposition of calcium hydroxide ($Ca(OH)_2$), is significantly lower. This can be explained by the fact that $Ca(OH)_2$ is consumed by the pozzolanic reaction of the fly ash. Since the $Ca(OH)_2$ content of FA0 is reduced to almost zero, it is also possible that FA0 contains undetermined amounts of primary, unreacted fly ash, which affects its usability as a concrete additive. Compared to FA0, S0 shows an increased mass loss at 500 °C, but this is lower than that of CEM. Since latent-hydraulic blast-furnace slag replaces 30 wt% of the CEM I here, less $Ca(OH)_2$ is produced in favor of calcium silicate hydrates

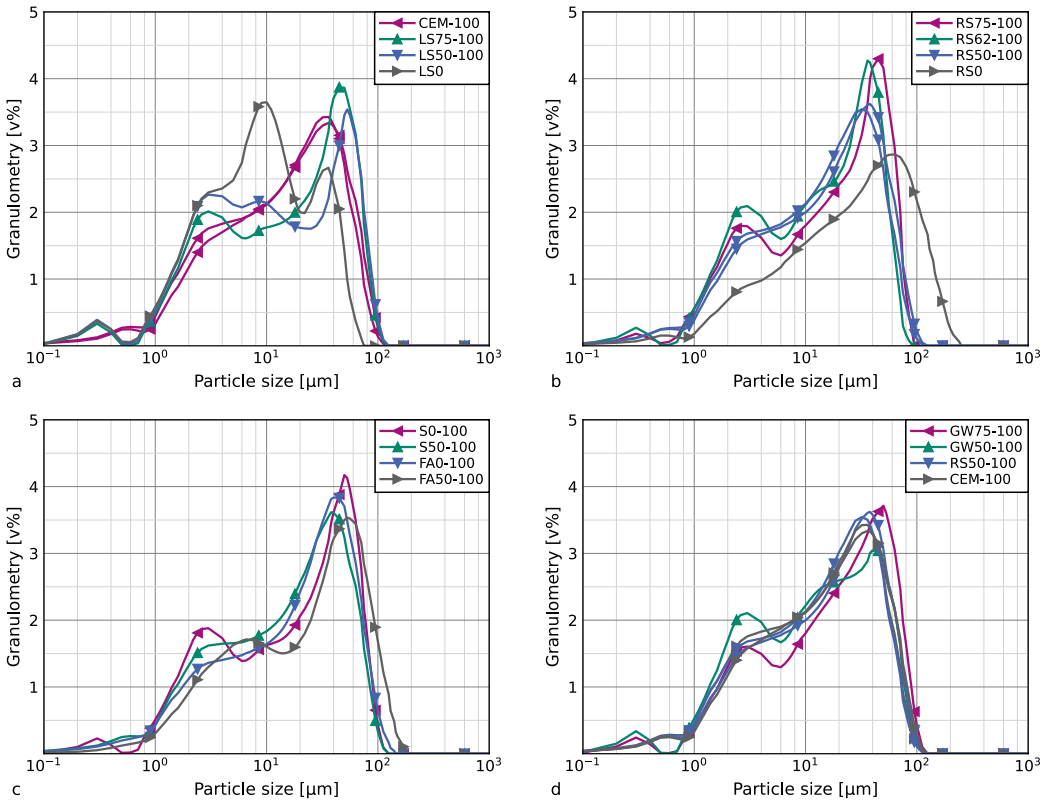


**Fig. 3.** Particle size distribution of ground artificial fines determined through laser diffraction.

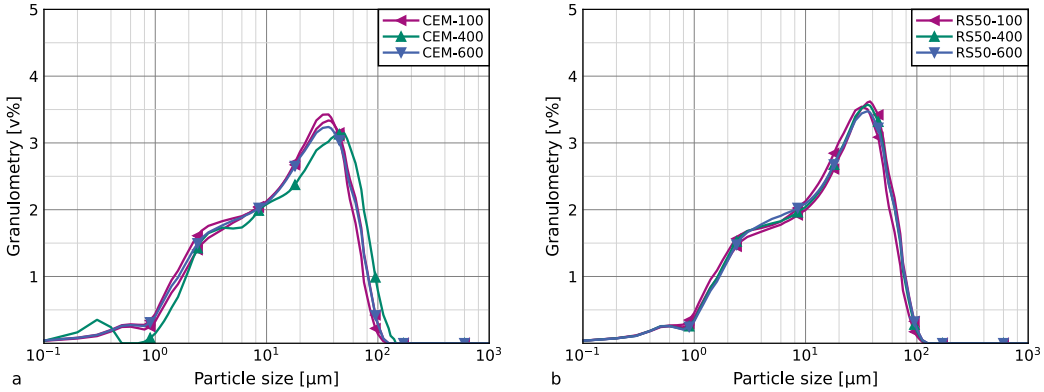


**Fig. 4.** Particle size distribution of artificial fines CEM and RS50 after thermal activation at different temperatures determined through laser diffraction.

(C–S–H) during hydration. This explains the increased mass loss at temperatures below 500 °C compared to CEM, which is mainly due to the decomposition of C–S–H.

The ultimate goal of using an industrial mill for grinding before thermal activation was to achieve good comparability between individual samples, allowing the exclusion of particle size influence on experimental results. Overall, ground artificial fines have similar particle size distributions, with the exception of LS0 and RS0, which is due to the diverging milling process (see Fig. 3).

To rule out the impact of thermal processing on particle size distribution, artificial fines CEM and RS50 were measured after processing at 400 °C and 600 °C. Laser diffraction measurements yielded no systematic influence of thermal activation on particle size, so the comprehensive determination of particle size distributions for all activated artificial fines combinations was forgone (see Fig. 4).

### 3.2. Artificial fines performance as SCM

#### 3.2.1. Hydration heat

The assessment of the rehydration behavior of processed artificial fines comprises four individual steps: The influence of activation temperature, the influence of paste content, the influence of aggregate composition, and, finally, the influence of CEM I-substitution rate.

The effect of the processing temperature on hydration heat development in Fig. 5 used three paste artificial fines (CEM, FA0, and S0) as well as mortar RS50 at a CEM I-substitution rate of 30 wt% in comparison to the average results from the eightfold determination of pure CEM I.

The results show a significant influence of the activation temperature for CEM: In the first minutes after water addition, the mixtures of CEM I with thermally activated CEM exhibit a significantly increased

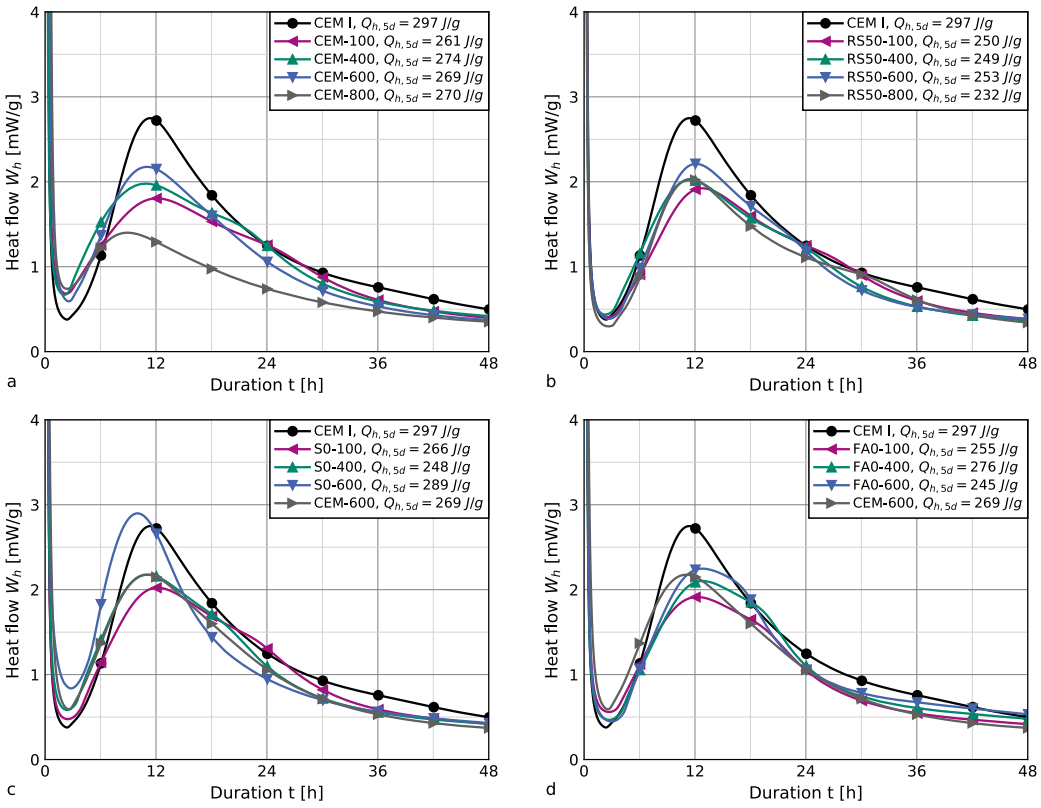


**Fig. 5.** Hydration heat development of blended binders with 70 wt% CEM I and 30 wt% artificial fines activated at different temperatures. See Table 2 for artificial fines composition.

heat release with rising temperature. Subsequently, the heat release decreases for all mixtures. Compared to pure CEM I, mixtures with all four processed CEM samples exhibit increased heat release during the induction period in the first 6 h of measurement. Subsequently, the curves show a flatter progression than the reference sample made of pure CEM I – the heat release is reduced depending on the processing temperature. CEM-600 shows the highest local maximum after the acceleration period, while the total heat released within 5 days between CEM-600 and CEM-400 hardly differs. CEM-100 exhibits the lowest hydration heat release. However, the behavior stemming from CEM-800 is particularly striking: Although only 30 wt% of CEM I was replaced, the initial heat release during the first 30 min increases by a factor of 4. The height of the local maximum of the hydration heat flow is reduced by about 50% and also occurs significantly earlier. Subsequently, the hydration heat flow curve of the mixture of CEM I and CEM-800 runs significantly flatter than that of the other investigated mixtures. Overall, none of the investigated mixtures of CEM I and thermally activated CEM reach the cumulative heat released by pure CEM I.

These observations are only partially transferable to RS50, although analogous tendencies are shown. The analysis is made more difficult by the fact that in the calorimetry measurements, reactive CEM I makes up 70 wt% of the solid quantity. Furthermore, RS50 consists of CEM I and river sand in a mass ratio of 0.46, so that the proportion of potentially reactivated cement paste in the solid quantity of the calorimetry balance is reduced from 30 wt% for CEM to 9.4 wt% for RS50. The hydration heat release is accordingly influenced to a lesser extent by the treatment temperature. The artificial fines RS50-100, RS50-400, and RS50-600 exhibit almost the same hydration heat release, with RS50-600 showing the highest local maximum, analogous to CEM-600. RS50-800 has a less pronounced effect on the hydration heat release compared to CEM-800, but results in a lower overall heat release than RS50-100. All mixtures of CEM I with thermally processed model materials RS50 release less heat cumulatively than the corresponding mixtures of CEM I with CEM.

Artificial fines whose cement paste matrix consists of hydration products of CEM I and blast-furnace slag (S0) or coal fly ash (FA0) show a behavior deviating from the processed CEM. Compared to CEM-600, the cumulative hydration heat release of S0-600 is significantly increased and reaches the level of pure CEM I, with the increased local maximum of the hydration heat flow being reached earlier (compare Baldusco et al., 2019; Xu et al., 2023b,a). S0-100 and S0-400 also show a slightly increased heat release compared to CEM-100 and CEM-400, respectively. However, the heat release in the first minutes after water addition is significantly reduced compared to CEM-600 and is similar to that of pure CEM I. The same applies to FA0, where, apart from the initial heat release in the first 24 h after water addition, no increased heat release is detectable. Subsequently, the processed materials, regardless of the activation temperature, exhibit an increased hydration heat flow.

Fig. 6(a) illustrates the corresponding results for artificial fines prepared at 600 °C with different contents of river sand. Here, a decrease in hydration heat release can be observed with decreasing cement paste content. However, further details cannot be inferred due to the scatter of the experimental results.

Fig. 6 shows the heat flow curves of artificial fines with different types of aggregate in comparison. The individual measurement results are close to each other, making interpretations difficult due to the scatter of the experimental results. On the one hand, it can be observed that the processing temperature has only a minor influence on the hydration heat release. The same applies to the type of aggregates. It can be seen that the artificial fines with 50 v% greywacke (GW50) show a reduced hydration heat release at the beginning of hydration, which is, however, compensated for in the further course. Artificial fines with 75 v% cement paste content show slightly increased cumulative hydration heat releases.

In Fig. 7, the results of hydration heat flow measurements on the processed artificial fines CEM-400, CEM-600, S0-600, and FA0-600 are

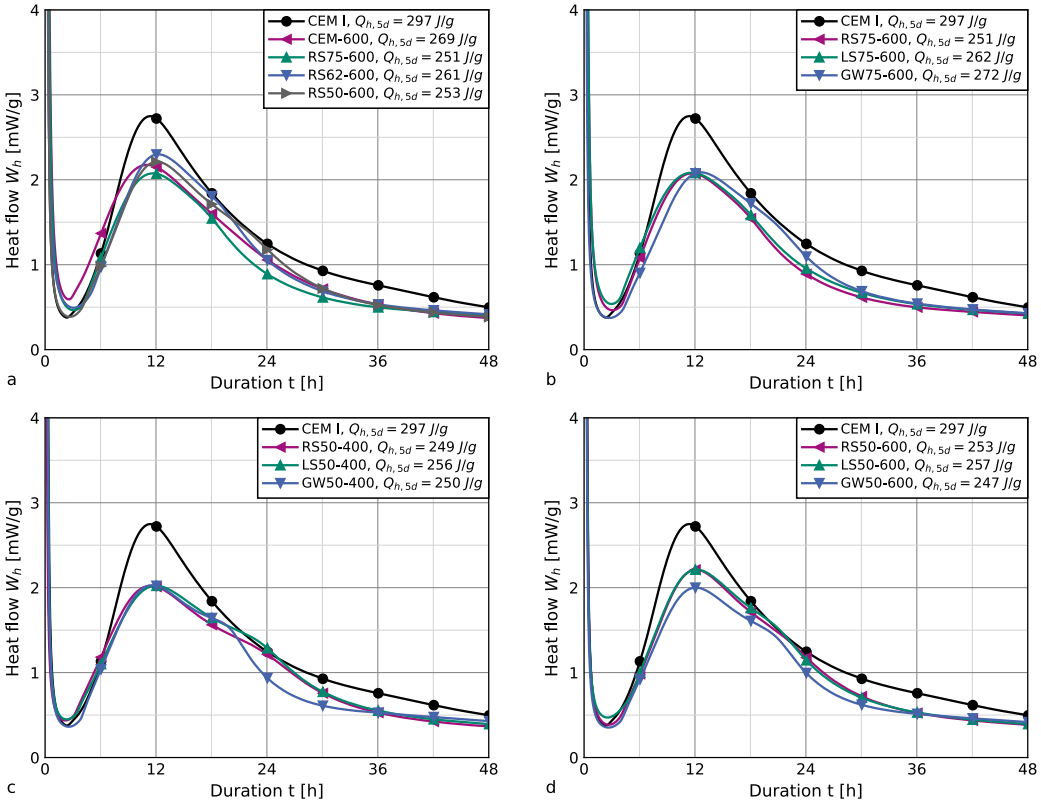


**Fig. 6.** Hydration heat development of select blends of 70 wt% CEM I and 30 wt% artificial fines with different aggregate contents and compositions, activated at 400 °C and 600 °C. See Table 2 for artificial fines composition.

compared for different substitution rates of CEM I (10 wt%, 30 wt%, 50 wt% and 100 wt%). The experimental results show, on the one hand, clear differences between the individual artificial fines among themselves, as well as between the substitution rates of respective processed artificial fines.

Activation of CEM at 400 °C produces a binder with hydraulic reactivity. The cumulative hydration heat release of pure CEM-400 corresponds to 55% of the heat release of CEM I after 5 d. Based on the results for pure CEM I, the hydration heat release decreases with increasing substitution rate. Considering the heat flows reveals a nuanced picture: CEM-400 releases more heat in the first minutes after water addition than CEM I. The difference stems from the near omission of the acceleration and deceleration phases between 2 h and 48 h present in CEM I-containing binder blends. While the heat flow of pure CEM-400 plateaus, blends with CEM I increase to a local maximum after an induction period with increased heat flow compared to CEM I. When replacing 50 wt% of CEM I with CEM-400, the hydration heat flow decreases more strongly after reaching the maximum than when replacing 30 wt%.

CEM-600 is also hydraulically reactive, with a cumulative hydration heat release after 5 d corresponding to 84% of CEM I. The difference to CEM-400 is approximately equal to the hydration heat release within the first hour after water addition. However, the heat flow of CEM-600, in contrast to CEM-400, shows a recognizable maximum after 10 h. Subsequently, the hydration heat flow decreases more strongly than that of CEM-400. Blends of CEM I and CEM-600 are arranged according to their replacement rates between the pure binders.

S0-600 also shows hydraulic reactivity, which is associated with a larger cumulative hydration heat release than CEM-600 and reaches 98% of the hydration heat of CEM I after 5 d. The evaluation of the hydration heat flows shows a more balanced course than CEM I, with a significantly increased local minimum after 3 h and a reduced and temporally shifted maximum after 15 h, so that the heat flow before the minimum and after the maximum is each higher than CEM I. The position of the minima and maxima of mixtures with 30 wt% and 50 wt% S0-600 is also changed, but no systematic relationship with the substitution rate can be identified.

When considering FA0-600, no hydraulic behavior is recognizable after the initial heat flow has subsided within the first hours after water addition. Only after several days does the hydration heat release increase measurably; a local maximum is reached after 163 h with $W_h = 0.4$ mW/g. The substitution of 30 wt% of CEM I through FA0-600 behaves similarly to corresponding blends containing CEM-600 and S0-600 except for a reduced initial hydration heat within the first minutes. The substitution of 50 wt% of CEM I through FA0-600 results in a reduced peak after the shortened acceleration phase and a plateauing deceleration phase.

In the overall view, the present results of the hydration heat flow measurements show a clear influence of the processing temperature, the binder composition, and, to a lesser extent, the aggregate content. Findings for the temperature-dependence agree with results in literature, where heat-release is partially attributed to the reaction of free lime as well as the reformation of calcium silicate hydrate and other hydrate phases (Angulo et al., 2022; Bogas et al., 2020; Semugaza et al., 2023; Real et al., 2020). The effect of hydration products from blast-furnace slag corroborates results presented in Baldusco et al. (2019), Xu et al. (2023b) and Xu et al. (2023a). Xu et al. (2023b) also reports a hydration heat release for a blended paste containing 30 wt% fly ash, which is considerably higher than the present results for FA0. However, the precursor in Xu et al. (2023b) contains a higher amount of $Ca(OH)_2$ compared to FA0, which supports the hypothesis of the importance of calcium hydroxide for fines rehydration. The effects observed here cannot be conclusively clarified with the available results, particularly the hypothesis of incomplete reaction of the fly ash in connection with the reduction of the $Ca(OH)_2$ content, as discussed in Section 3.1. The type of aggregate is of lesser importance for the hydration heat

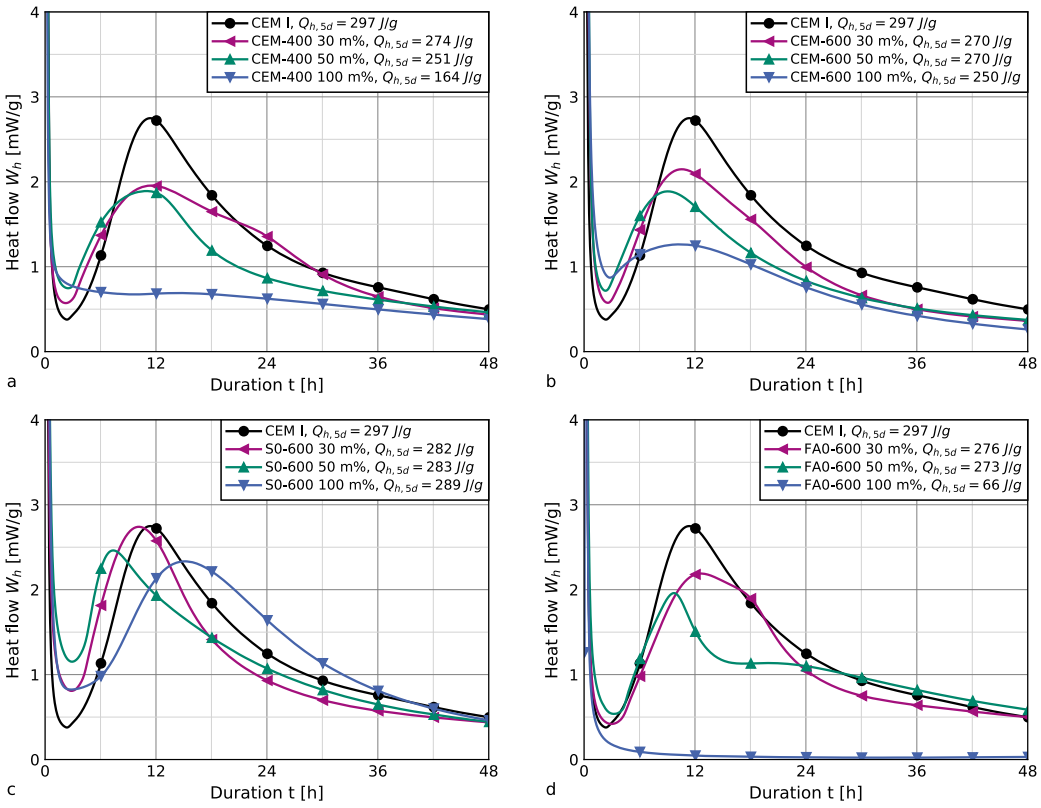


**Fig. 7.** Hydration heat flow of select blends of CEM I and CEM-400, CEM-600, S0-600 or FA0-600 at different substitution rates. See Table 2 for artificial fines composition.

release, while the general presence of inert particles generally reduces the hydration heat release, which agrees with previous findings for limestone-blended cement pastes (Serpell and Lopez, 2013; Xu et al., 2023b). The ratio of CEM I to thermally activated artificial fines brings additional effects that overlap and interact with the previously mentioned factors (compare Zhang et al., 2018).

### 3.2.2. Compressive strength development

To analyze the strength development of the manufactured mortar mixtures, two approaches were used. The quotient $r$ according to Eq. (1) describes the ratio of the mortar compressive strength at the ages of 2 d and 28 d, and was determined for all mixtures.

$$r = \frac{f_{c,2\,\mathrm{d}}}{f_{c,28\,\mathrm{d}}} \tag{1}$$

Fig. 8 shows results for the mortar compressive strength $f_c$ at the age of 2 d and 28 d for different compositions in which thermo-mechanically activated model fines partially substitute CEM I. The quotient in the present representation is illustrated through lines of different slopes. The mortar compressive strength at the age of 28 d, which in turn strongly depends on the SCM content and the $w/b$-ratio, significantly influences $r$, which increases with higher $f_{c,28\,\mathrm{d}}$. For similar $f_{c,28\,\mathrm{d}}$, artificial fines activated at 400 °C or 600 °C exhibit similar $r$, while increasing activation temperature to 800 °C leads to reduced $r$ and mortar with artificial fines processed at 100 °C show increased $r$. These results mirror findings in literature, where compressive strength development of dehydrated cement paste is similar to Portland cement up to 3 d, but falls behind at later ages (Bogas et al., 2020; Real et al., 2020).

The resulting values for $r$ correspond to the results for CEM I-mortar with different $w/c$-ratios (here, respective mean values from three series). These range from $r = 0.46$ for $w/c = 0.60$ (with $f_{c,28\,\mathrm{d}} = 40.4$ MPa) to $r = 0.50$ for $w/c = 0.55$ (with $f_{c,28\,\mathrm{d}} = 48.0$ MPa) and

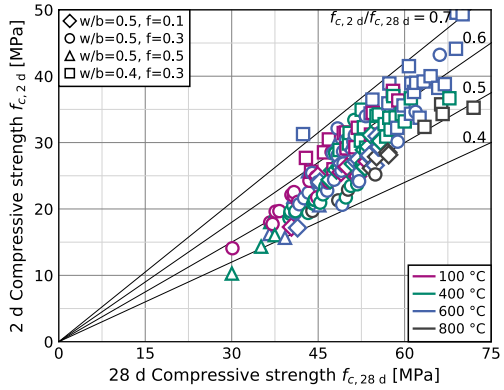


**Fig. 8.** Mortar compressive strength $f_c$ at the age of 2 d over mortar compressive strength at 28 d for different mixes with partial CEM I-substitution through processed artificial fines. Marker shapes indicate mix composition, and colors indicate the activation temperature. (For interpretation of the references to color in this figure legend, the reader is referred to the web version of this article.)

$r = 0.51$ for $w/c = 0.50$ (with $f_{c,28\,\mathrm{d}} = 53.3$ MPa) to $r = 0.62$ for $w/c = 0.45$ (with $f_{c,28\,\mathrm{d}} = 56.3$ MPa).

Additionally, Eq. (2) was adapted from fib Model Code (2023) and adjusted to the results of mixtures that were tested at the ages of 1 d, 2 d, 7 d and 28 d using the least squares method.

$$f_c(t) = \beta_{cc}(t) \cdot f_{c,28\,\mathrm{d}} \quad \text{with} \tag{2}$$

$$\beta_{cc}(t) = \exp\left\{ s_c \cdot \left[ 1 - \left( \frac{28}{t} \right)^{l} \right] \right\} \tag{3}$$

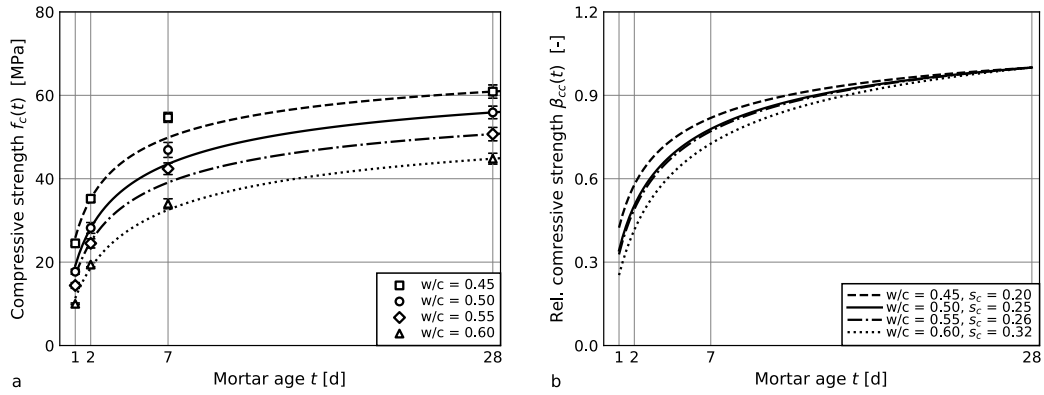


**Fig. 9.** Temporal compressive strength development (absolute (a) and relative (b)) of CEM I-mortar with different w/c ratio at the age of 1 d, 2 d, 7 d and 28 d, (mean and standard deviation from six prism halves for each data point as well as regression curves following Eq. (2)).

The parameter $l = 0.5$ is independent of the binder. A global analysis showed that these results in an underestimation of the strength development of the examined mortars at the age of 7 d. $l = 0.85$ would allow a better overall fit to the experimental data. However, for the following evaluation of the activated artificial fines, $l = 0.5$ was applied to enable better comparison with the values given in fib Model Code (2023). Subsequently, the parameter $s_c$ was calculated for each individual mixture.

Fig. 9 illustrates the results for $f_c(t)$ and $\beta_{cc}(t)$, which were measured or calculated for mortars with CEM I with different $w/c$-ratios. The expected increase in compressive strength with decreasing $w/c$-ratios was shown, as well as a faster initial strength development with increasing strength. The calculated parameters $s_c$ using regression analysis lie between 0.20 for $w/c = 0.45$ and 0.32 for $w/c = 0.60$. Thus, the values for $s_c$ correspond to the values in fib Model Code (2023) of 0.3 and 0.2 for CEM I 42,5 R for characteristic concrete compressive strength $f_{ck} \leq 35$ MPa and 35 MPa $< f_{ck} <$ 60 MPa, respectively.

In Fig. 10, the corresponding calculated curves of $\beta_{cc}(t)$ are shown for eight mixtures with CEM I-substitution by thermally activated artificial fines ($f = 0.3$ at $w/b = 0.50$). The artificial fines CEM, RS75, RS62, and RS50 were used as SCMs, which were thermally activated at 400 °C or 600 °C. Strength tests were performed at the age of 1 d, 2 d, 7 d and 28 d on three prisms each. The replacement of CEM I by activated artificial fines generally leads to decreasing strengths at the age of 28 d. Apart from this, the relative temporal strength development, illustrated by the time functions $\beta_{cc}(t)$, is not affected. The determined values for $s_c$ range from 0.19 for RS62-400 to 0.32 for RS75-600, with no systematic influence of activated artificial fines composition. Activation at 800 °C exhibits similar, yet slightly increased results for $s_c$, with $s_c = 0.32$ for CEM-800 and $s_c = 0.30$ for RS75-800, indicating a decelerated strength development.

### 3.2.3. Compressive strength at 28 d

The analysis of the test results regarding the influence of using processed artificial fines on the mortar compressive strength at the age of 28 d was based on the so-called $k$-value concept, which is described in CEN/TR 16639:2014. In this approach, the $w/b$-ratio (Eq. (4)) is replaced by an equivalent water-cement ratio $(w/c_{eq})$ according to Eq. (5). The $k$-values serve as a measure of the reactivity of the supplementary cementitious materials and thus as an indication of their influence on the compressive strength. The European concrete standard EN 206:2017 defines $k$-values for individual types of SCM, such as $k = 0.4$ for fly ash or $k = 0.6$ for blast-furnace slag.

$$\frac{w}{b} = \frac{w}{c + a} \quad \text{with } a\text{: mass of (reactive) SCMs} \tag{4}$$

$$\frac{w}{c_{eq}} = \frac{w}{c + k \cdot a} \tag{5}$$

Rather than the application of preset values for $k$ to produce concrete with a target compressive strength, the present research uses Eq. (5) to calculate $k$-values for all activated artificial fines individually. Subsequently, $k$-values can serve as a measure for the analysis of the reactivity and compressive strength contribution of mode materials composition. Essential for determining equivalent water-cement ratios is the knowledge of the relationship between compressive strength $f_c$ and the water-cement ratio $w/c$, which was first established for the 14 base mixtures from three series without SCMs (see Fig. 11).

For further computation, the test results were approximated using regression curves based on the least squares method. While normally convex curves are used for analyzing this material behavior, the present data are best represented by a linear approach (Eq. (6)), which is also proposed in CEN/TR 16639:2014.

$$f_{c,28\,d} = \alpha - \beta \cdot \frac{w}{c} \quad \text{with } \alpha = 105 \text{ and } \beta = 106 \tag{6}$$

The subsequent calculation of $k$ uses the measured compressive strength to compute the corresponding equivalent water-cement ratio $w/c_{eq}$ (Eq. (7)). With the additional input of mix parameters (substitution rate $f$ and the water-binder ratio $w/b$), Eq. (8) gives the individual $k$-value of a specific mortar mix.

$$\frac{w}{c_{eq}} = \frac{\alpha - f_{c,28\,d}}{\beta} \tag{7}$$

$$k = 1 - \frac{1}{f} \cdot \left(1 - \frac{w/b}{w/c_{eq}}\right) \tag{8}$$

To evaluate the $k$-values of the mixtures with processed artificial fines as SCMs, it is first investigated to what extent the binder content $f$ and the water-binder ratio $w/b$ influence the overall results. For this purpose, pairs of mixtures from a sample set are considered. For $w/b = 0.50$, 37 successful test pairs are available, which result in arithmetic means of $k(f = 0.1) = 1.07$ and $k(f = 0.3) = 0.65$, suggesting an influence of the SCM content on the analysis results. 53 test pairs for $f = 0.3$ yield $k\,(w/b = 0.40) = 0.72$ and $k\,(w/b = 0.50) = 0.68$, whereby the influence of the water-binder ratio on the calculated $k$-values can be considered negligible.

Therefore, in the next step, these 53 test pairs for $f = 0.3$ were used to determine influencing factors of processing parameters as well as artificial fines composition. Fig. 12 illustrates the arithmetic mean values of the 53 test pairs.

By comparing the artificial fines CEM, LS75, and LS50 (Fig. 12(a)), it becomes apparent that the treatment temperature only indirectly influences the reactivity. Instead, the mass loss due to dehydration is the decisive criterion for the reactivity resulting from thermal processing. CEM activated at 400 °C (CEM-400) shows a similar mass loss of $\Delta m = 9.4$ wt% as LS75-600 with $\Delta m = 9.7$ wt%, resulting in $k = 0.66$ for both artificial fines (mean values over two test pairs). LS75-400 and

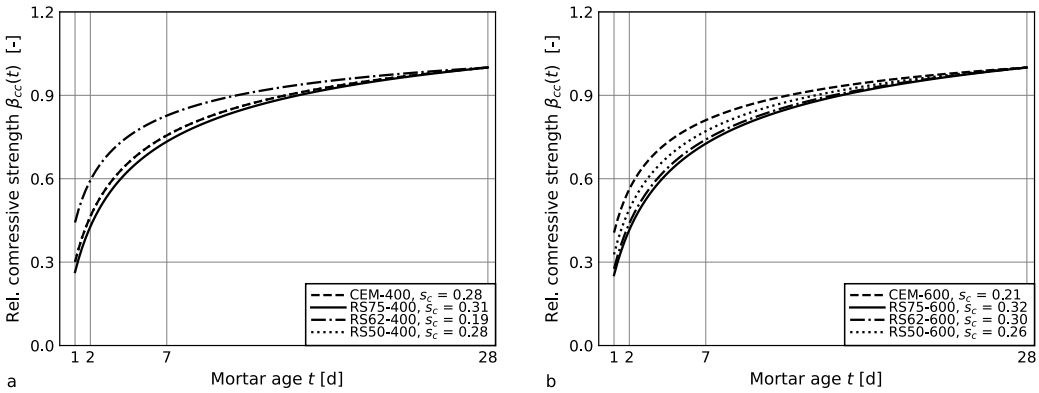


**Fig. 10.** Relative temporal compressive strength development of mortar containing artificial fines with different river sand content activated at 400 °C (a) and 600 °C (b).

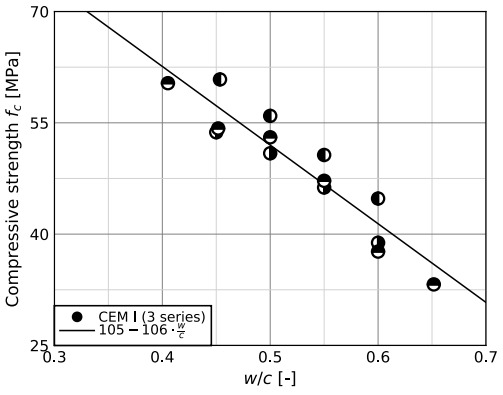


**Fig. 11.** Relationship between compressive strength $f_c$ and water-cement ratio for mortar mixes without CEM I-substitution for $0.40 \leq w/c \leq 0.65$.

LS50-600 behave similarly (with an outlier due to material scattering being plausible). For all examined test series with the artificial fines CEM, LS75, LS50, and LS0, a linear relationship between $k$ and $\Delta m$ can be observed. A plausible deviation is CEM-800 with $\Delta m = 18.0\,\mathrm{wt\%}$, as the mass loss can only be attributed to dehydration up to processing temperatures of approximately 650 °C, after which the decomposition of carbonates with the release of $CO_2$ begins (Klingsch, 2014). The high $k$-values for thermally activated CEM corroborate findings in Bogas et al. (2022a), Carriço et al. (2020b), Letelier et al. (2017), Ma et al. (2022), Qian et al. (2020), Tokareva et al. (2023), Vashistha et al. (2023) and Wu et al. (2023), where the substitution of Portland cement through thermally activated cement paste has only minor negative effects on compressive strength. Paste precursors containing limestone powder, which is similar to LS75, exhibit reduced strength (Xu et al., 2023b; Serpell and Lopez, 2013).

When considering artificial fines with river sand instead of limestone as aggregate (Fig. 12(b)), a slight increase in $k$-values can be observed, regardless of the mass loss. The same applies more pronouncedly to artificial fines with greywacke (Fig. 12(d)). Ground limestone (or limestone powder) acts as an inert SCM, whereas $SiO_2$ from the aggregate contained in the artificial fines can exhibit pozzolanic reactivity. Prerequisites for this are that $SiO_2$ is amorphous or that crystalline quartzitic $SiO_2$ has been very finely ground. While it can be assumed that artificial fines with river sand and greywacke contain some particles with sufficient fineness, greywacke also contains amorphous $SiO_2$.

Additional positive effects on the reactivity of thermally activated artificial fines become apparent when they contain reaction products of blast-furnace slag or fly ash (Fig. 12(c)), which corroborates findings in Xu et al. (2023b,a).

Based on these observations, various model approaches are subsequently investigated to predict $k$-values based on the artificial fines composition and mass loss during thermal processing. The analysis is based on 49 test pairs with a CEM I-substitution rate of $f = 0.3$ through artificial fines processed at 100 °C, 400 °C or 600 °C.

The best fit is defined in Eq. (9). Model parameters are determined using the method of least squares from 98 individual results of the 49 test pairs with $f = 0.3$. As a result, the sum of the squared errors amounts to $\Delta^2 = 14.8$ and the coefficient of determination for the compressive strength is $R^2 = 0.75$. The results are illustrated in Fig. 13.

$$k = k_h \cdot \Delta m + k_a + k_b \tag{9}$$

$$k_h = 5.70 \tag{10}$$

$$k_a = \begin{cases} 0.00 & \text{for LS} \\ 0.10 & \text{for RS} \\ 0.30 & \text{for GW} \end{cases} \tag{11}$$

$$k_b = \begin{cases} 0.15 & \text{for CEM I} \\ 0.30 & \text{for CEM I + S} \\ 0.45 & \text{for CEM I + FA} \end{cases} \tag{12}$$

For ground artificial fines, the $k$-value comprises a binder-dependent and an aggregate-dependent constant parameter. The mass loss $\Delta m$ during thermal activation increases $k$ linearly. Alongside the interpretation of $\Delta m$ as chemically bound water, $k_h$ can be transformed into the amount of water bound per unit-weight of cement, $m_h$ (see Eq. (13)). $k_h = 5.70$ corresponds to $m_h = 0.21$. Despite the indirect determination method, this agrees with the amount of chemically bound water from Power's model (Powers and Brownyard, 1946; Brouwers, 2004; Lura et al., 2017).

$$k_h = 1 + \frac{1}{m_h} \tag{13}$$

A simplified model, where artificial fines composition is not accounted for ($k_a = k_b = 0.00$) yields an increased $k_h = 8.80$ at a higher sum of the squared errors ($\Delta^2 = 20.4$) and a reduced coefficient of determination for the compressive strength ($R^2 = 0.40$). Similarly, when using the exact artificial fines composition to alter Eq. (9) to directly account for the aggregate and paste content, the sum of squared errors increases slightly to $\Delta^2 = 14.9$. The coefficient of determination for the compressive strength decreases insignificantly ($R^2 = 0.73$).

Subsequently, an extension of Eq. (9) for $k$ to account for the CEM I-substitution rate ($f$) is investigated. The best approach (Eq. (14)) yields $R^2 = 0.77$ (starting from $R^2 = 0.75$ without considering $f$).

$$k = (k_h \cdot \Delta m + k_a + k_b) \cdot \left(\frac{f_{ref}}{f}\right)^{k_f} \tag{14}$$

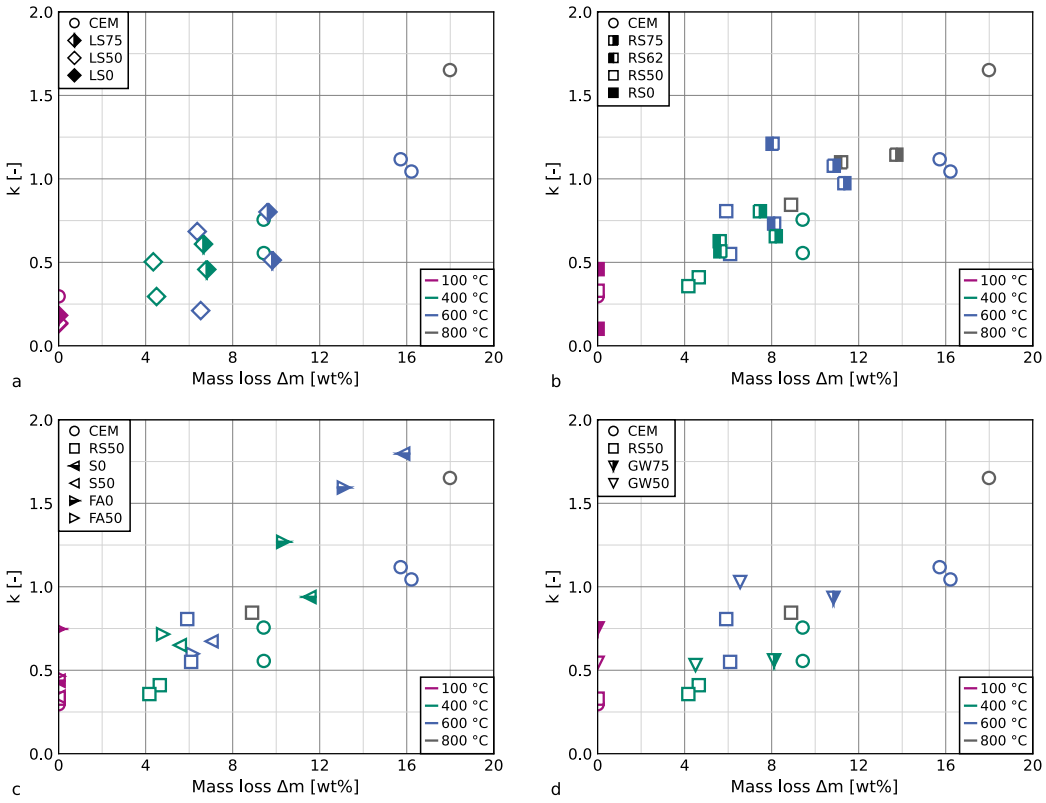


**Fig. 12.** Relationship between $k$-values of processed artificial fines and mass loss during thermal activation (arithmetic means for $w/b = 0.40$ and $w/b = 0.50$ at $f = 0.3$).

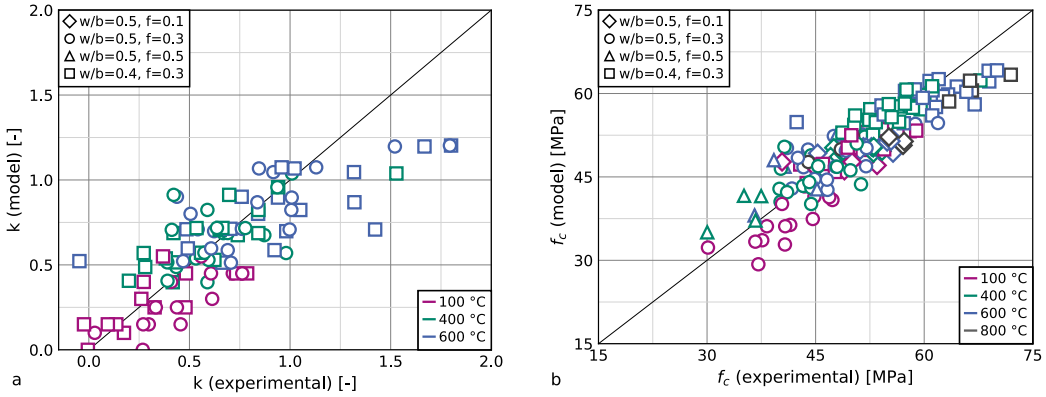


**Fig. 13.** Modeled over measured $k$-values for $f = 0.3$ (a), modeled over measured compressive strength $f_c$ for all mix compositions (b).

$$k_f = 0.5 \tag{15}$$

$f_{ref}$ denotes the CEM I-substitution rate for which the basic model was calibrated; presently $f_{ref} = 0.3$. The nonetheless relatively poor model fit is due to incomplete data: For $f = 0.1$, no experiments were conducted with the artificial fines S0, S50, FA0, and FA50. For $f = 0.5$, the scope of the experiments was further significantly reduced, making it impossible to analyze the influence of the binder content in conjunction with some artificial fines parameters. Furthermore, the results for $f = 0.1$ are subject to significantly increased scatter, which results from the calculation procedure (see Eq. (8)). Fig. 14 confirms that the scatter of theoretical $k$-values increases with decreasing substitution rate $f$, since all material scatter is projected onto a decreasing proportion of the binder. Nevertheless, it becomes apparent that the model adaptation leads to a significantly improved prediction of the $k$-value, in that $k$-values for $f = 0.1$ are no longer underestimated and for $f = 0.5$ are no longer overestimated. However, only the latter has a notable influence on the prediction of the mortar compressive strength, since a cement substitution of 10 wt% generally only shows minor effects on compressive strength.

## 4. Conclusions

The present results detail the impact of concrete fines composition on compressive strength contribution after thermal activation. The substitution of 30 wt% OPC through pure cement paste activated at 600 °C does not affect compressive strength ($k = 1.0$). When cement paste contains hydration products from blast-furnace slag or fly ash, compressive strength at 28 d can even exceed the reference ($k > 1.0$). Compressive strength contribution decreases with increasing aggregate content in the fines, but also depends on the aggregate composition, with limestone sand performing worse than quartzitic sand.

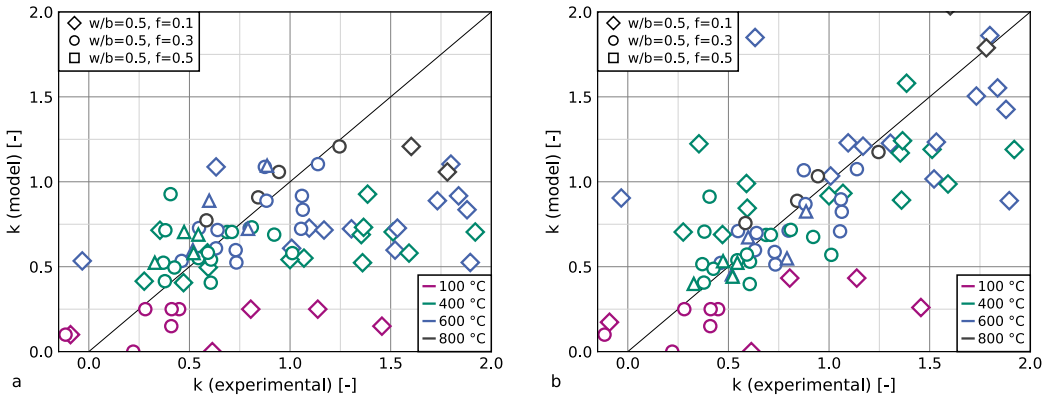


**Fig. 14.** Modeled $k$-values without consideration of the substitution rate $f$ (a) and with consideration of $f$ through Eq. (14) (b).

Fines containing greywacke with amorphous silicates exhibit increased compressive strength contribution, even without thermal activation.

While the activation temperature remains the most important processing parameter for achieving high compressive strength, the present analysis finds an overall good correlation between mass loss during thermal activation and compressive strength contribution, regardless of fines composition and aggregate content. The proposed model for strength contribution is based on the $k$-value approach in EN:206:2017 and reflects binder and aggregate composition through fixed parameters. The linear influence of the mass loss agrees with theoretical assumptions for the chemically bound water content in hardened cement paste.

While these findings are mostly based on a CEM I-substitution of 30 wt%, a model extension reflects findings from both the present experimental work as well as literature, where compressive strength contribution reduces with increasing substitution rate. This allows for increasing compressive strength when up to 10 wt% of CEM I is substituted through thermally activated concrete fines.

The temporal compressive strength development of mortar containing thermally activated concrete fines is independent of their composition or processing temperature. Overall, besides the aforementioned impact on absolute strength, relative strength development is similar to CEM I. Only when fines are processed at 800 °C, relative strength development slows.

High early strength is caused by fast rehydration of fines, which exhibit an increased and accelerated hydration heat development during the first 6 h after mixing. While fines composition has a minor impact on hydration heat development, results for different substitution rates suggest interactions between activated fines and Portland cement, which require additional research.

While the proposed model for strength contribution has been calibrated for the extensive present experimental data, an industrial application requires an even broader dataset, which includes cement, SCMs, and aggregates from different geographical sources, with a more detailed analysis of their compositions. This dataset may then serve as a benchmark and model validation for industrially processed concrete fines, where the composition is generally unknown. As the present analysis focuses on compressive strength, further studies also require the investigation of concrete durability and the applicability of empirical provisions in structural design codes.

## CRediT authorship contribution statement

**Jan P. Höffgen:** Writing – original draft, Visualization, Methodology, Funding acquisition, Formal analysis, Conceptualization. **Frank Dehn:** Writing – review & editing, Supervision, Project administration, Funding acquisition.

## Declaration of Generative AI and AI-assisted technologies in the writing process

During the preparation of this work the authors used Grammarly and DeepL in order to check for spelling and wording errors. After using these tools/services, the authors reviewed and edited the content as needed and take full responsibility for the content of the published article.

## Funding

This work was supported by the Dres. Edith und Klaus Dyckerhoff-Stiftung, grant no. T0218/36374.

## Declaration of competing interest

The authors declare that they have no known competing financial interests or personal relationships that could have appeared to influence the work reported in this paper.

## Acknowledgments

The authors would like to thank Jakob Grigo and Jonas Vormschlag for their invaluable experimental work.

## Data availability

Data will be made available on request.

## References

Alonso, C., Fernandez, L., 2004. Dehydration and rehydration processes of cement paste exposed to high temperature environments. J. Mater. Sci. 39 (9), 3015–3024. http://dx.doi.org/10.1023/B:JMSC.0000025827.65956.18.

Angulo, S.C., Guilge, M.S., Quarcioni, V.A., Cincotto, M.A., Nobre, T.R., Pöllmann, H., 2022. The role of calcium silicates and quicklime on the reactivity of rehydrated cements. Constr. Build. Mater. 340, 127625. http://dx.doi.org/10.1016/j.conbuildmat.2022.127625.

Aquino Rocha, J.H., Toledo Filho, R.D., 2023. The utilization of recycled concrete powder as supplementary cementitious material in cement-based materials: A systematic literature review. J. Build. Eng. 76, 107319. http://dx.doi.org/10.1016/j.jobe.2023.107319.

Baggio, T.F., Possan, E., De Oliveira Andrade, J.J., 2024. Physical-chemical characterization of construction and demolition waste powder with thermomechanical activation for use as supplementary cementitious material. Constr. Build. Mater. 437, 136907. http://dx.doi.org/10.1016/j.conbuildmat.2024.136907.

Baldusco, R., Nobre, T.R.S., Angulo, S.C., Quarcioni, V.A., Cincotto, M.A., 2019. Dehydration and rehydration of blast furnace slag cement. J. Mater. Civ. Eng. 31 (8), 04019132. http://dx.doi.org/10.1061/(ASCE)MT.1943-5533.0002725.

Baquerizo, L.G., Matschei, T., Scrivener, K.L., 2016. Impact of water activity on the stability of ettringite. Cem. Concr. Res. 79, 31–44. http://dx.doi.org/10.1016/j.cemconres.2015.07.008.

Barthel, M., Rübner, K., Kühne, H.-C., Rogge, A., Dehn, F., 2016. From waste materials to products for use in the cement industry. Adv. Cem. Res. 28 (7), 458–468. http://dx.doi.org/10.1680/jadcr.15.00149.

Bogas, J.A., Carriço, A., Pereira, M., 2019. Mechanical characterization of thermal activated low-carbon recycled cement mortars. J. Clean. Prod. 218, 377–389. http://dx.doi.org/10.1016/j.jclepro.2019.01.325.

Bogas, J.A., Carriço, A., Real, S., 2022a. Durability of concrete produced with recycled cement from waste concrete. Mater. Today: Proc. 58, 1149–1154. http://dx.doi.org/10.1016/j.matpr.2022.01.280.

Bogas, J.A., Carriço, A., Tenza-Abril, A.J., 2020. Microstructure of thermoactivated recycled cement pastes. Cem. Concr. Res. 138, 106226. http://dx.doi.org/10.1016/j.cemconres.2020.106226.

Bogas, J.A., Real, S., Carriço, A., Abrantes, J., Guedes, M., 2022b. Hydration and phase development of recycled cement. Cem. Concr. Compos. 127, 104405. http://dx.doi.org/10.1016/j.cemconcomp.2022.104405.

Brameshuber, W., Hannawald, J., Hauer, B., Herbst, T., Meng, B., Nebel, H., Pierkes, R., Rübner, K., Schäfer, S., Seidel, M., Vollpracht, A., DAfStb, 2011. Verbundforschungsvorhaben nachhaltig bauen mit beton: potenziale des sekundärstoffeinsatzes im betonbau - teilprojekt b effiziente sicherstellung der umweltverträglichkeit von beton - teilprojekt e. DAfStb-Heft, vol. 584, Beuth, Berlin.

Brouwers, H., 2004. The work of powers and Brownyard revisited: Part 1. Cem. Concr. Res. 34 (9), 1697–1716. http://dx.doi.org/10.1016/j.cemconres.2004.05.031.

Carriço, A., Bogas, J.A., Guedes, M., 2020a. Thermoactivated cementitious materials – a review. Constr. Build. Mater. 250, 118873. http://dx.doi.org/10.1016/j.conbuildmat.2020.118873.

Carriço, A., Bogas, J.A., Hu, S., Real, S., Costa Pereira, M.F., 2021a. Novel separation process for obtaining recycled cement and high-quality recycled sand from waste hardened concrete. J. Clean. Prod. 309, 127375. http://dx.doi.org/10.1016/j.jclepro.2021.127375.

Carriço, A., Real, S., Bogas, J.A., 2021b. Durability performance of thermoactivated recycled cement concrete. Cem. Concr. Compos. 124, http://dx.doi.org/10.1016/j.cemconcomp.2021.104270.

Carriço, A., Real, S., Bogas, J.A., Costa Pereira, M.F., 2020b. Mortars with thermo activated recycled cement: Fresh and mechanical characterisation. Constr. Build. Mater. 256, 119502. http://dx.doi.org/10.1016/j.conbuildmat.2020.119502.

Chen, L., Wei, M., Lei, N., Li, H., 2024. Effect of chemical–thermal activation on the properties of recycled fine powder cementitious materials. Case Stud. Constr. Mater. 20, e02956. http://dx.doi.org/10.1016/j.cscm.2024.e02956.

Coffetti, D., Crotti, E., Gazzaniga, G., Carrara, M., Pastore, T., Coppola, L., 2022. Pathways towards sustainable concrete. Cem. Concr. Res. 154, 106718. http://dx.doi.org/10.1016/j.cemconres.2022.106718.

Cyr, M., Diliberto, C., Lecomte, A., Izoret, L., 2019. Recycled concrete as cement main constutient (CMC) or supplementary cementitious materials (SCM). In: Larrard, F.c., Colina, H. (Eds.), Concrete Recycling: Research and Practice. CRC Press/Taylor & Francis Group, Boca Raton, FL, pp. 83–95.

fib Model Code, 2023. fib model code for concrete structures (2020), Version 1. In: International Federation for Structural Concrete (Ed.), International Federation for Structural Concrete (fib), Lausanne, ISBN: 978-2-88394-175-5.

Florea, M.V.A., 2014. Secondary Materials Applied in Cement-Based Products : Treatment, Modelling and Environmental Interaction (Ph.D. thesis). Technische Universiteit Eindhoven, http://dx.doi.org/10.6100/IR772902.

Frías, M., Martínez-Ramírez, S., La Villa, R.V., Fernández-Carrasco, L., García, R., 2021. Reactivity in cement pastes bearing fine fraction concrete and glass from construction and demolition waste: microstructural analysis of viability. Cem. Concr. Res. 148, 106531. http://dx.doi.org/10.1016/j.cemconres.2021.106531.

Friol Guedes de Paiva, F., Tamashiro, J.R., Pereira Silva, L.H., Kinoshita, A., 2021. Utilization of inorganic solid wastes in cementitious materials – a systematic literature review. Constr. Build. Mater. 285, 122833. http://dx.doi.org/10.1016/j.conbuildmat.2021.122833.

Gao, Y., Schutter, G., Ye, G., Yu, Z., Tan, Z., Wu, K., 2013. A microscopic study on ternary blended cement based composites. Constr. Build. Mater. 46, 28–38. http://dx.doi.org/10.1016/j.conbuildmat.2013.04.021.

Ge, P., Song, Y., Quan, J., Wu, Y., Zhou, J., 2024. Study on the activity, phase, thermal decomposition characteristics, microstructure, and chemical element of hardened cement powder under heating temperature of 100°c˜1200°c. Struct. Concr. http://dx.doi.org/10.1002/suco.202301108.

Gebremariam, A.T., Di Maio, F., Vahidi, A., Rem, P., 2020. Innovative technologies for recycling End-of-Life concrete waste in the built environment. Resour. Conserv. Recycl. 163, 104911. http://dx.doi.org/10.1016/j.resconrec.2020.104911.

Hafez, H., Kurda, R., Cheung, W.M., Nagaratnam, B., 2020. Comparative life cycle assessment between imported and recovered fly ash for blended cement concrete in the UK. J. Clean. Prod. 244, 118722. http://dx.doi.org/10.1016/j.jclepro.2019.118722.

Herrmann, A., Koenig, A., Dehn, F., 2018. Structural concrete based on alkali-activated binders: terminology, reaction mechanisms, mix designs and performance. Struct. Concr. 19 (3), 918–929. http://dx.doi.org/10.1002/suco.201700016.

Horváth, I., Proks, I., Nerád, I., 1977. Activation energies of the thermal decompositions of C3AH6 AND C3AD6 by the isothermal TG method. J. Therm. Anal. 12 (1), 105–110. http://dx.doi.org/10.1007/BF01909862.

Izoret, L., Diliberto, C., Mechling, J.M., Lecomte, A., Natin, P., 2019. Recycled concrete sand as alternative raw material for Portland clinker production. In: Larrard, F.c., Colina, H. (Eds.), Concrete Recycling: Research and Practice. CRC Press/Taylor & Francis Group, Boca Raton, FL, pp. 63–81.

Kim, J.-H., Seo, E.-A., Kim, D.-G., Chung, C.-W., 2021. Utilization of recycled cement powder as a solidifying agent for radioactive waste immobilization. Constr. Build. Mater. 289, 123126. http://dx.doi.org/10.1016/j.conbuildmat.2021.123126.

Kim, J., Ubysz, A., 2024. Thermal activation of multi-recycled concrete powder as supplementary cementitious material for repeated and waste-free recycling. J. Build. Eng. 98, 111169. http://dx.doi.org/10.1016/j.jobe.2024.111169.

Klingsch, E.W., 2014. Explosive Spalling of Concrete in Fire (Ph.D. thesis). ETH Zurich, Zürich, http://dx.doi.org/10.3929/ethz-a-010243000.

Knight, K.A., Cunningham, P.R., Miller, S.A., 2023. Optimizing supplementary cementitious material replacement to minimize the environmental impacts of concrete. Cem. Concr. Compos. 139, 105049. http://dx.doi.org/10.1016/j.cemconcomp.2023.105049.

Letelier, V., Tarela, E., Muñoz, P., Moriconi, G., 2017. Combined effects of recycled hydrated cement and recycled aggregates on the mechanical properties of concrete. Constr. Build. Mater. 132, 365–375. http://dx.doi.org/10.1016/j.conbuildmat.2016.12.010.

Li, S., Gao, J., Li, Q., Zhao, X., 2021. Investigation of using recycled powder from the preparation of recycled aggregate as a supplementary cementitious material. Constr. Build. Mater. 267, 120976. http://dx.doi.org/10.1016/j.conbuildmat.2020.120976.

Liang, C., Zhang, Y., Wu, R., Yang, D., Ma, Z., 2021. The utilization of active recycled powder from various construction wastes in preparing ductile fiber-reinforced cementitious composites: A case study. Case Stud. Constr. Mater. 15, 00650. http://dx.doi.org/10.1016/j.cscm.2021.e00650.

Lipowsky, A., Müller, A., 2017. Gesteinsmehl als Zuschlagstoffe in hydraulischen Bindemitteln. Aufbereitungs-Technik/Mineral Process. 58 (12), 52–64.

Liu, Q., Xiao, J., Singh, A., 2021. Quantification of plastic shrinkage and cracking in mortars containing different recycled powders using digital image correlation technique. Constr. Build. Mater. 293, 123509. http://dx.doi.org/10.1016/j.conbuildmat.2021.123509.

Lura, P., Winnefeld, F., Fang, X., 2017. A simple method for determining the total amount of physically and chemically bound water of different cements. J. Therm. Anal. Calorim. 130 (2), 653–660. http://dx.doi.org/10.1007/s10973-017-6513-z.

Ma, Z., Shen, J., Wu, H., Zhang, P., 2022. Properties and activation modification of eco-friendly cementitious materials incorporating high-volume hydrated cement powder from construction waste. Constr. Build. Mater. 316, 125788. http://dx.doi.org/10.1016/j.conbuildmat.2021.125788.

Ma, Z., Wu, Y., Fang, K., Zhang, Y., Wang, C., 2025. Developing fully recycled alkali-activated mortar made with waste concrete fines as a substitute for both binder and sand: multi-properties evaluation. Constr. Build. Mater. 477, 141323. http://dx.doi.org/10.1016/j.conbuildmat.2025.141323.

Müller, C., Dora, B., 2000. Verwertung von brechsand aus bauschutt. Deutscher Ausschuss Für Stahlbeton, vol. 506, Beuth, Berlin.

Noel, N., Mielke, T., Semugaza, G., Gierth, A.Z., Helmich, S., Nawrath, S., Lupascu, D.C., 2025. Chemical transformations during the preparation and rehydration of reactivated virgin cements. CEMENT 19, 100129. http://dx.doi.org/10.1016/j.cement.2025.100129.

Ohemeng, E.A., Ekolu, S.O., 2020. A review on the reactivation of hardened cement paste and treatment of recycled aggregates. Mag. Concr. Res. 72 (10), 526–539. http://dx.doi.org/10.1680/jmacr.18.00452.

Powers, T.C., Brownyard, T.L., 1946. Studies of the physical properties of hardened portland cement paste. ACI J. Proc. 43 (9), 249–336. http://dx.doi.org/10.14359/15301.

Qian, D., Yu, R., Shui, Z., Sun, Y., Jiang, C., Zhou, F., Ding, M., Tong, X., He, Y., 2020. A novel development of green ultra-high performance concrete (UHPC) based on appropriate application of recycled cementitious material. J. Clean. Prod. 261, 121231. http://dx.doi.org/10.1016/j.jclepro.2020.121231.

Real, S., Carriço, A., Bogas, J.A., Guedes, M., 2020. Influence of the treatment temperature on the microstructure and hydration behavior of thermoactivated recycled cement. Materials 13 (18), 3937. http://dx.doi.org/10.3390/ma13183937.

Richardson, I.G., 2000. The nature of the hydration products in hardened cement pastes. Cem. Concr. Compos. 22 (2), 97–113. http://dx.doi.org/10.1016/S0958-9465(99)00036-0.

Schneider, U., 1982. Verhalten von Beton bei hohen temperaturen. DAfStb-Heft, vol. 337, Wilhelm Ernst und Sohn, Berlin.

Scrivener, K.L., Juilland, P., Monteiro, P.J., 2015. Advances in understanding hydration of Portland cement. Cem. Concr. Res. 78, 38–56. http://dx.doi.org/10.1016/j.cemconres.2015.05.025.

Semugaza, G., Mielke, T., Castillo, M.E., Gierth, A.Z., Tam, J.X., Nawrath, S., Lupascu, D.C., 2023. Reactivation of hydrated cement powder by thermal treatment for partial replacement of ordinary portland cement. Mater. Struct. 56 (3), http://dx.doi.org/10.1617/s11527-023-02133-9.

Serpell, R., Lopez, M., 2013. Reactivated cementitious materials from hydrated cement paste wastes. Cem. Concr. Compos. 39, 104–114. http://dx.doi.org/10.1016/j.cemconcomp.2013.03.020.

Serpell, R., Lopez, M., 2015. Properties of mortars produced with reactivated cementitious materials. Cem. Concr. Compos. 64, 16–26. http://dx.doi.org/10.1016/j.cemconcomp.2015.08.003.

Serpell, R., Zunino, F., 2017. Recycling of hydrated cement pastes by synthesis of α′H-C2S. Cem. Concr. Res. 100, 398–412. http://dx.doi.org/10.1016/j.cemconres.2017.08.001.

Shah, I.H., Miller, S.A., Jiang, D., Myers, R.J., 2022. Cement substitution with secondary materials can reduce annual global CO2 emissions by up to 1.3 gigatons. Nat. Commun. 13 (1), 5758. http://dx.doi.org/10.1038/s41467-022-33289-7.

Shen, P., Sun, Y., Liu, S., Jiang, Y., Zheng, H., Xuan, D., Lu, J., Poon, C.S., 2021. Synthesis of amorphous nano-silica from recycled concrete fines by two-step wet carbonation. Cem. Concr. Res. 147, 106526. http://dx.doi.org/10.1016/j.cemconres.2021.106526.

Shui, Z., Xuan, D., Wan, H., Cao, B., 2008. Rehydration reactivity of recycled mortar from concrete waste experienced to thermal treatment. Constr. Build. Mater. 22 (8), 1723–1729. http://dx.doi.org/10.1016/j.conbuildmat.2007.05.012.

Snellings, R., Suraneni, P., Skibsted, J., 2023. Future and emerging supplementary cementitious materials. Cem. Concr. Res. 171, 107199. http://dx.doi.org/10.1016/j.cemconres.2023.107199.

Sousa, L.N., Zepper, J., Schollbach, K., Brouwers, H., 2024. Improving the reactivity of industrial recycled concrete fines: exploring mechanical and hydrothermal activation. Constr. Build. Mater. 442, 137594. http://dx.doi.org/10.1016/j.conbuildmat.2024.137594.

Sui, Y., Ou, C., Liu, S., Zhang, J., Tian, Q., 2020. Study on properties of waste concrete powder by thermal treatment and application in mortar. Appl. Sci. 10 (3), 998. http://dx.doi.org/10.3390/app10030998.

Sun, C., Chen, L., Xiao, J., Singh, A., Zeng, J., 2021. Compound utilization of construction and industrial waste as cementitious recycled powder in mortar. Resour. Conserv. Recycl. 170, 105561. http://dx.doi.org/10.1016/j.resconrec.2021.105561.

Tajuelo Rodriguez, E., Garbev, K., Merz, D., Black, L., Richardson, I.G., 2017. Thermal stability of C-S-H phases and applicability of Richardson and Groves' and richardson C-(A)-S-H(I) models to synthetic C-S-H. Cem. Concr. Res. 93, 45–56. http://dx.doi.org/10.1016/j.cemconres.2016.12.005.

Tokareva, A., Kaassamani, S., Waldmann, D., 2023. Fine demolition wastes as supplementary cementitious materials for CO2 reduced cement production. Constr. Build. Mater. 392, 131991. http://dx.doi.org/10.1016/j.conbuildmat.2023.131991.

Vashistha, P., Oinam, Y., Kim, H.-K., Pyo, S., 2023. Effect of thermo-mechanical activation of waste concrete powder (WCP) on the characteristics of cement mixtures. Constr. Build. Mater. 362, 129713. http://dx.doi.org/10.1016/j.conbuildmat.2022.129713.

VDZ, 2024. Environmental Data of the German Cement Industry 2023. Tech. rep., Verein Deutscher Zementwerke e.V., Düsseldorf.

Wang, J., Lacarrière, L., Sellier, A., 2019. Multicomponent modelling of cement paste dehydration under different heating rates. Mater. Struct. 52 (1), 6. http://dx.doi.org/10.1617/s11527-018-1306-9.

Wang, C., Zhang, Z., Liu, X., Zhang, Y., Ma, Z., 2024. Elucidating the role of recycled concrete aggregate in ductile engineered geopolymer composites: Effects of recycled concrete aggregate content and size. J. Build. Eng. 95, 110150. http://dx.doi.org/10.1016/j.jobe.2024.110150.

Wei, M., Chen, L., Lei, N., Li, H., Huang, L., 2024. Experimental investigation on freeze–thaw resistance of thermally activated recycled fine powder concrete. Constr. Build. Mater. 457, 139378. http://dx.doi.org/10.1016/j.conbuildmat.2024.139378.

Wei, M., Chen, L., Lei, N., Li, H., Huang, L., 2025. Mechanical properties and microstructures of thermally activated ultrafine recycled fine powder cementitious materials. Constr. Build. Mater. 475, 141195. http://dx.doi.org/10.1016/j.conbuildmat.2025.141195.

Wiedmann, A., 2020. Schadensrisiko und Schadensentwicklung in Betonfahrbahndecken als Folge einer Alkali-Kieselsäure-Reaktion. KIT-Bibliothek, Karlsruhe, http://dx.doi.org/10.5445/IR/1000125632.

Wu, H., Liang, C., Zhang, Z., Yao, P., Wang, C., Ma, Z., 2023. Utilizing heat treatment for making low-quality recycled aggregate into enhanced recycled aggregate, recycled cement and their fully recycled concrete. Constr. Build. Mater. 394, 132126. http://dx.doi.org/10.1016/j.conbuildmat.2023.132126.

Wu, H., Liu, X., Wang, C., Zhang, Y., Ma, Z., 2024. Micro-properties and mechanical behavior of high-ductility engineered geopolymer composites (EGC) with recycled concrete and paste powder as green precursor. Cem. Concr. Compos. 152, 105672. http://dx.doi.org/10.1016/j.cemconcomp.2024.105672.

Xi, X., Zheng, Y., Du, C., Zhang, P., Sun, M., 2024a. Study on the hydration characteristics, mechanical properties, and microstructure of thermally activated low-carbon recycled cement. Constr. Build. Mater. 447, 138042. http://dx.doi.org/10.1016/j.conbuildmat.2024.138042.

Xi, X., Zheng, Y., Zhuo, J., Zhang, P., Golewski, G.L., Du, C., 2024b. Influence of water glass modulus and alkali content on the properties of alkali-activated thermally activated recycled cement. Constr. Build. Mater. 452, 138867. http://dx.doi.org/10.1016/j.conbuildmat.2024.138867.

Xu, L., Wang, J., Li, K., Hao, T., Li, Z., Li, L., Ran, B., Du, H., 2023a. New insights on dehydration at elevated temperature and rehydration of GGBS blended cement. Cem. Concr. Compos. 139, 105068. http://dx.doi.org/10.1016/j.cemconcomp.2023.105068.

Xu, L., Wang, J., Li, K., Li, M., Lin, S., Hao, T., Wang, T., Guo, Y., Ling, Z., 2023b. Investigations on the rehydration of recycled blended SCMs cement. Cem. Concr. Res. 163, 107036.

Xu, L., Wang, J., Li, K., Lin, S., Li, M., Hao, T., Ling, Z., Xiang, D., Wang, T., 2022. A systematic review of factors affecting properties of thermal-activated recycled cement. Resour. Conserv. Recycl. 185, 106432. http://dx.doi.org/10.1016/j.resconrec.2022.106432.

Yonis, A., Oinam, Y., Vashistha, P., Degefa, A.B., Belayneh, G.B., Park, S., Pyo, S., 2024. Novel activation method of waste concrete powder for sustainable clinker-free binder. Cem. Concr. Compos. 151, 105600. http://dx.doi.org/10.1016/j.cemconcomp.2024.105600.

Yu, R., Shui, Z., 2013. Influence of agglomeration of a recycled cement additive on the hydration and microstructure development of cement based materials. Constr. Build. Mater. 49, 841–851. http://dx.doi.org/10.1016/j.conbuildmat.2013.09.004.

Zelic, J., Ugrina, L., Jozic, D., 2007. Application of thermal methods in the chemistry of cement: Kinetic Analysis of Portlandite from non-isothermal thermogravimetric data. In: The First International Proficiency Testing Conference. n. d., Sinaia, Romania, pp. 420–429.

Zhang, L., Yongsheng, J., Guodong, H., Li, J., Hu, Y., 2018. Modification and enhancement of mechanical properties of dehydrated cement paste using ground granulated blast-furnace slag. Constr. Build. Mater. (164), 525–534. http://dx.doi.org/10.1016/j.conbuildmat.2017.12.232.

Zhang, H., Zhang, B., Tang, L., Zeng, W., 2023. Analysis of two processing techniques applied on powders from recycling of clay bricks and concrete, in terms of efficiency, energy consumption, and cost. Constr. Build. Mater. 385, 131517. http://dx.doi.org/10.1016/j.conbuildmat.2023.131517.

Zheng, Y., Xi, X., Liu, H., Du, C., Lu, H., 2024. A review: enhanced performance of recycled cement and CO2 emission reduction effects through thermal activation and nanosilica incorporation. Constr. Build. Mater. 422, 135763. http://dx.doi.org/10.1016/j.conbuildmat.2024.135763.

Zhou, Q., Glasser, F.P., 2001. Thermal stability and decomposition mechanisms of ettringite at <120°c. Cem. Concr. Res. 31 (9), 1333–1339. http://dx.doi.org/10.1016/S0008-8846(01)00558-0.

Zhou, Q., Lachowski, E.E., Glasser, F.P., 2004. Metaettringite, a decomposition product of ettringite. Cem. Concr. Res. 34 (4), 703–710. http://dx.doi.org/10.1016/j.cemconres.2003.10.027.